International Journal of Environmental Sciences
ISSN: 2229-7359
Vol. 11 No. 22s, 2025
https://theaspd.com/index.php

Optical and gamma radiation shield studies on Bi_2O_3-B_2O_3-Fe_2O_3- $Bi_{3.25}Dy_{0.75}Ti_3O_{12}$ glass-matrices

Aafreen Sultana[1], Md. Shareefuddin[1], G. Ramadevudu[2] and N. V. Prasad[2*]
[1]Material research laboratory[1], Department of Physics, Osmania University, Hyderabad-07, India
[2]Department of Physics, Vasavi College of Engineering, Ibrahimbagh, Hyderabad-31, India.
Corresponding author E-mail: nvp1969@rediffmail.com

Abstract:
The present ceramic-embedded glass matrix samples (100-x) [0.7 Bi_2O_3-0.2B_2O_3-0.1Fe_2O_3] + x [$Bi_{3.25}Dy_{0.75}Ti_3O_{12}$]; named as (100-x) BBF + x (BDT), with x=30,40,50,60 mol%, were prepared by traditional melt–quench method. The XRD spectroscopy revealed the amorphous nature and with increasing the $Bi_{3.25}Dy_{0.75}Ti_3O_{12}$ (BDT), it partially tuned to the mixed (crystalline-amorphous) structure. The density and molar volume values were found to increase with increasing the concentration of BDT, whereas the oxygen packing fraction decreases with an increase in the ferroelectric (BDT) concentration. Detailed optical spectroscopic measurements were carried out on BBF-BDT samples. FTIR Spectroscopy clearly confirms the presence of tri and tetra borate units. Raman spectroscopic analysis was also made to understand the optical and dielectric modes. Radiation shielding properties were studied and MAC (mass attenuation coefficient) values were found to be high (97.2cm^2/gm-6.3cm^2/gm) in the energy range of 0.01 MeV to 0.1 MeV). Small peaks observed in the intermediate energy range (0.06 Mev) confirms the mixed nature of the sample. All the samples were observed to be opaque in nature. The optical band gap was found to decrease with the BDT concentration. The results were corroborated by the optical and radiation shielding parameters. Based on the metallization criteria, it is concluded that these materials would be useful for non-linear optical applications. In addition, theoretical radiation shielding parameters are in good argument with the reported values. This suggests that this glass-matrix may be used in gamma radiation absorbers is considered to be environmental protective monitoring matrix systems.

1. INTRODUCTION

Glass-ceramics are the most widely probed materials for their capability to propose both amorphous and crystalline phases [1-4]. Their combined properties have become favourable in a particular field of optoelectronic applications. One can tune these materials by controlling the structural parameters like size of the crystal, the volume fraction of the crystalline phase, etc. Amongst all ferroelectrics, $Bi_4Ti_3O_{12}$ (BT) of the Aurivillius family is an eminent lead-free bismuth layered structure ferroelectric (BLSF) material. It is reported that the rare-earth modified BT has shown potential applications in display integrated chips, solid-state lasers and opto-electronic devices [5,6]. The structure of this compound consists of alternate bismuth oxide layers $(Bi_2O_2)^{2+}$ with perovskite blocks $(A_{m-1}B_mO_{3m+1})^{2-}$. The term 'm' represents the number of perovskite blocks present in the layer structure. In the present case, m=3, A is a tri-valent ion (Bi/Dy) with 12-coordinated cation. The term B represents cation (Ti) with 6-coordinated cation. In addition, rare-earth modified BIT has shown fast switching speed, large remnant polarization (P_r), high fatigue resistance, high dielectric constant, large spontaneous polarization and high curie temperature (675^0C) [7,8]. Based on the literature study as well as our recent results, it proves that the incorporation of rare-earth ions in bismuth site not only improves ferroelectric nature but also minimizes the secondary or mixed phases like $Bi_2Ti_2O_7$ and $Bi_{12}TiO_{20}$ [9-13]. On the other hand, mixed bismuth-borate glasses have profoundly influenced the field of glass ceramics due to their excellent optical properties like high refractive index, high density and high infrared transparency, which promotes its applications in non-linear optics and radiation shielding fields [14-16]. In addition to this, these oxide glasses have high phonon energy and better mechanical properties [17,18]. The glass system Bi_2O_3 – B_2O_3 with Fe_2O_3 at higher concentrations acts as a network modifier with high thermal stability within the vicinity of the boro-bismuth glass network [19]. The radiation shielding theoretical-studies on glass-materials are increased owing to the fact of its inheriting optical properties. Based on the results, one can use these materials as bio-radiation absorbers [20].

In view of the aforementioned importance of both the glass-network and the ferroelectric system, we have chosen a Fe_2O_3 based boro-bismuth glass network, namely B_2O_3-Bi_2O_3-Fe_2O_3 and Dy modified bismuth titanate [$Bi_{3.75}Dy_{0.25}Ti_3O_{12}$] ferroelectric system. The ferroelectric glass composition of (100-x) BBF+ x (DBT), where x = 30, 40, 50 and 60 wt.% was synthesized by a melt-quenching method. The glass-matrices were studied for their structural, morphological, optical and radiation-shielding properties.

2. Experimental procedure

The glass composition of 70 Bi_2O_3 – 20B_2O_3-10Fe_2O_3 (BBF) was prepared by taking the appropriate amounts of Bi_2O3, $B_2O_3$and Fe_2O_3. The mixture was ground for several hours. Prior to this, we prepared the ferroelectric material BDT ($Bi_{3.25}Dy_{0.75}Ti_3O_{12}$) by taking oxide powders of Bi_2O_3 (99.9% purity), Dy_2O_3 (>99.9% purity) and (TiO_2) (>99% purity) in the required amount and were hand-grinded in agate mortar, and ball milled with ethanol for 12 hours. Then, the powder-mixture was dried under the IR-lamp and sintered at 850°C in the porcelain crucible with a lid-covered, to prevent evaporation of bismuth oxide. The sintered powder was again hand ground in agate mortar for 6 hours and the phase of this powder was characterized by X-ray diffraction with Cukα radiation. The XRD reports revealed the single phase of DBT. Finally, the chosen glass-matrix composition of (100-x) [BBF} + x [DBT], with x=30, 40,50, 60 mol% was prepared by taking the wt.% powders of BBF and DBT. The glass and ferroelectric powders were mixed and heated at 1200 – 1250^{0}C for half an hour in a non -reactive porcelain crucibles with lid and the molten viscous fluid were quickly quenched by pouring it onto the preheated stainless-steel plate and pressed with another plate (maintained at nearly 100^{0}C). The list of the glass matrix samples prepared in this work along with the named code is given in Table 1.

S.NO.	x-BDT (wt. %) ($Bi_{3.25}Dy_{0.75}Ti_3O_{12}$)	(100-x) BBF [wt.%] (Bi_2O_3-B_2O_3.Fe_2O_3)	Sample code
1.	30	70	BDT30 + BBF70
2.	40	60	BDT40 + BBF60
3.	50	50	BDT50 + BBF50
4.	60	40	BDT60 + BBF40

Table –1 Composition of prepared x BDT+ (100-x) BBF (x=30, 40, 50 and 60) glass- matrix samples and their code

X-ray diffraction measurements were recorded on the glass-matrix samples, using Pan Analytic X'pert plus diffractometer, with Cu-kα (1.54 Å) radiation. The density of the samples was measured using the Archimedes principle using xylene as a liquid medium. Scanning electron micrograms and elemental analysis were obtained with EDS (Electron dispersive spectroscopy) attached ZEISSEVO18 microscope. Fourier transformation infrared (FTIR) spectra were recorded using FTIR-8400S in the range of 400-2000 cm-1. Optical absorption studies were made using UV-VIS 3092 spectrometer. Raman spectra were recorded, using a laser wavelength of 785 nm, with a Horiba Jobin Yvon Raman spectrometer.

The theoretical-studies on the effect of gamma radiation on these materials were made and discussed, using Phy-X program. This computer software runs on different parameters and within different given energies. The parameters like Z_{eff}, mean free path (MFP), linear attenuation coefficient (LAC) and mass attenuation coefficient (MAC) were simulated in the photon energy range (0.015eV-15Mev).

3. RESULTS AND DISCUSSIONS:

X-ray diffraction of the prepared of BDT-BBF glass-matrix with different compositions was recorded for 2 in the range of $10^0 \leq \Theta \leq 80^0$, shown in Fig.1 (a-e). Fig. 1e shows the XRD pattern of ferroelectric material (DBT). All the Bragg peaks were indexed based on the parent compound $Bi_4Ti_3O_{12}$. From the Fig 1 it is evident that the preferred orientation characteristic odd miller indices (1 1 3), (1 1 5) and (1 1 7) were found to merge and become a broad peak nature. This is a clear indication of the mixed or intergrowth nature of the BLSF-mixed phases [11]. A shift of broad peak towards the lower Bragg angle, with increasing the BDT concentration in the glass-matrix implies that the BDT phase gets dispersed and diffused into the glass matrix. The presence of Dy and Bi ions also contributes to the dispersed or mixed intergrowth

phases. Moreover, the appearance of the prominent peak (1 3 7) near 56° of Bragg angle is consideredas the characteristic peak for the orthorhombic structure. From this it is clarified that the more concentration of BDT fabricated glass matrix (Fig. 1d) consists of both glass and crystalline structures.From this it is clarified that the more concentration of BDT fabricated glass matrix (Fig. 1d) consists of both glass and crystalline structures. However, they belong to amorphous and hence are treated as glass-matrices only. It should be pointed out here that amongst $Bi_{4-x}Dy_xTi_3O_{12}$ ceramics, x=0.75 (BDT) has shown high

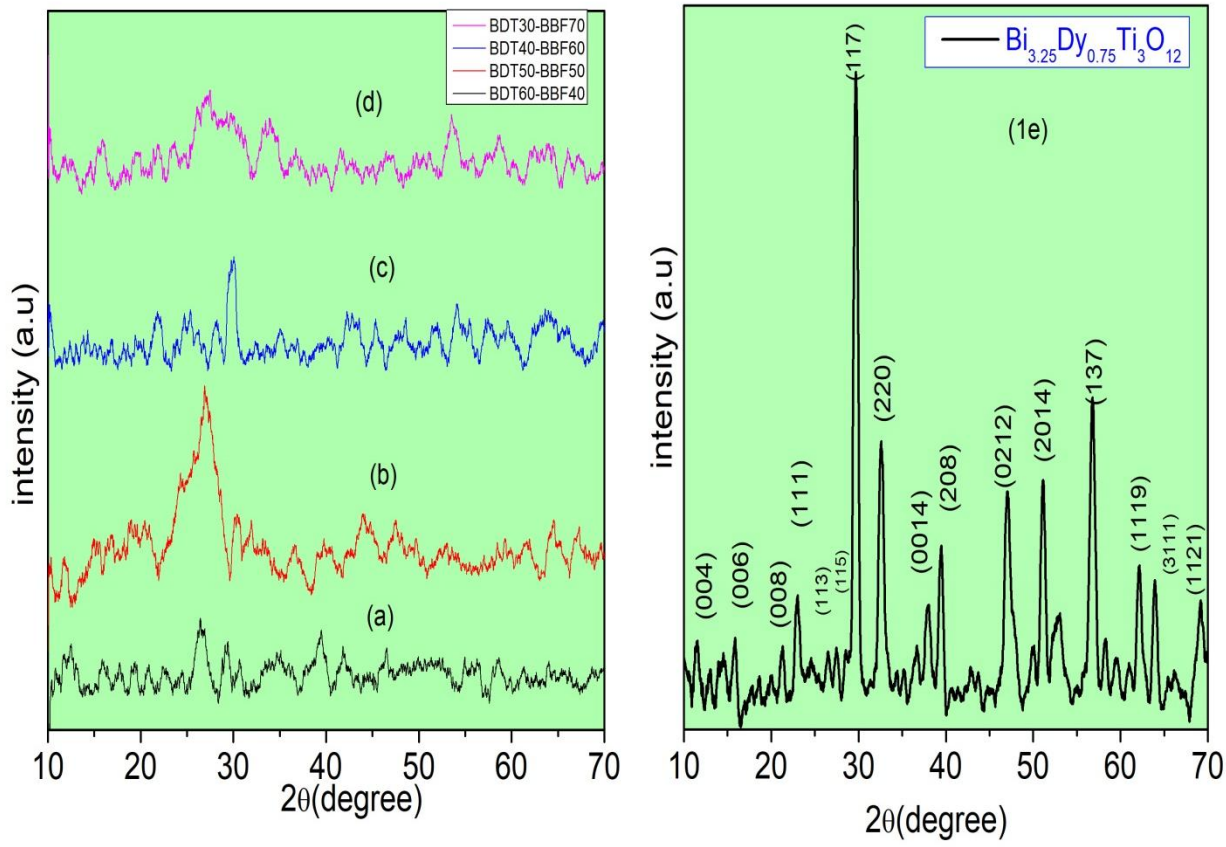

Fig 1 (a-d) XRD plots of (100-x) BBF+ x (DBT), where x = 30, 40, 50 and 60 wt.%

density, minimized volatile nature of bismuth ions. The structural change is also ascribed to the ionic radius (r), where the radius of Dy and Bi is within the tolerance of Hume-Rothery condition ($r_{Dy^{3+}}$ = 0.912 Å and $r_{Bi^{3+}}$ =1.03 Å).

The density and molar volume of transition metal ion concentration (N_i), Polaron radius (r_0), interionic distance (R) and oxygen packing density (OD) values were calculated from the following equations:

Density of the samples were calculated from the Archimedes Principle,

$$\rho = \frac{W_a}{W_a - W_b} * \rho_b \qquad (1)$$

Where ρ_b is the density of the reference liquid (xylene=0.865 g/cc). The terms W_a & W_b represent the weight of the glass-ceramic samples measured in air and xylene respectively. Molar volume can be calculated by the relation,

$$V_m = \frac{M_c}{\rho} \qquad (2)$$

M_C is the molecular weight of the glass-ceramic. Transition metal ion concentration (N) can be calculated by using the relation,

$$N = \frac{0.01 * N_a * \rho}{V_m} \qquad (3)$$

Where N_A is Avogadro number and ρ is density and V_m are molar volume of the samples respectively. Polaron radius of the glass matrix is calculated by using the formula:

$$r_p = \left(\frac{1}{N}\right)^{1/3} \quad (4)$$

Here, N represents the transition metal ion concentration. The interionic distance of the constituent atoms is calculated by using the formula:

$$r_i = \frac{1}{2}(\pi/6N)^{\frac{1}{3}} \quad (5)$$

The above said calculation was made and summarized in Table 2.

Table 2: Density (ρ), Molar volume (V_m), Transition metal ion concentration (N), Polaron radius (r_p), Inter ionic distance (r_i), Oxygen packing density (OPD), Optical band gap (E_{opt}) and Urbach Energy (Eg) of (100-x) BBF- x DBT (x= 30, 40, 50 and 60 wt.%) glass matrixes

From Table 2, it is evident that the density is found to increase with increasing the BDT concentration or decreasing the BBF glass concentration. This is due to the low relative molecular mass, compared to

S.no	Sample Code	Density (gm/cc)	Molar Volume (cc/mol)	Transition metal ion concentration (N_i) /cc	Polaron radius (r_p) (Å)	Interionic distance (r_i) (Å)	Oxygen Packing Density (OPD) g. atm/L	E_{opt} (eV)	Urbach energy (eV)
1	BDT30 + BBF70	6.14	92.5	$3.99x10^{20}$	1.36	5.47	227.02	1.80	0.14
2	BDT40 + BBF60	6.18	102.73	$3.62x10^{20}$	1.40	5.65	204.42	1.85	0.12
3	BDT50 + BBF50	6.11	115.46	$3.17x10^{20}$	1.46	5.91	181.88	1.83	0.12
4	BDT60 + BBF40	6.38	120.46	$3.19x10^{20}$	1.46	5.89	174.323	1.72	0.125

Bi_2O_3 or BDT. It is reported that the bismuth-borate network possesses long chains of BiO_6 distorted voids linked with Bi-O-Bi bonds [21-23]. The molar volume of the glasses follows the same trend. The increasing nature of the molar volume is attributed to the conversion of bridging oxygen (BO) to non-Bridging oxygen atoms (NBO) in the glass matrix and could be due to the increase in the bismuth ions or BDT which acts as network modifier. Molar volume is found to increase with increasing the BDT content in the

glass matrix. This data supports the XRD by showing sharp odd indexed peaks, namely (1 3 7) and (1 1 19) at higher Bragg angles.

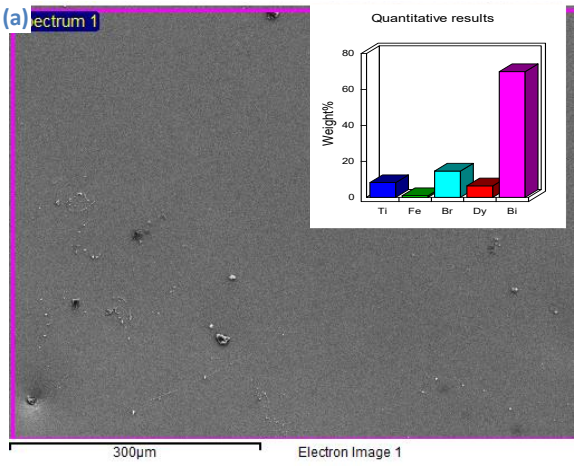

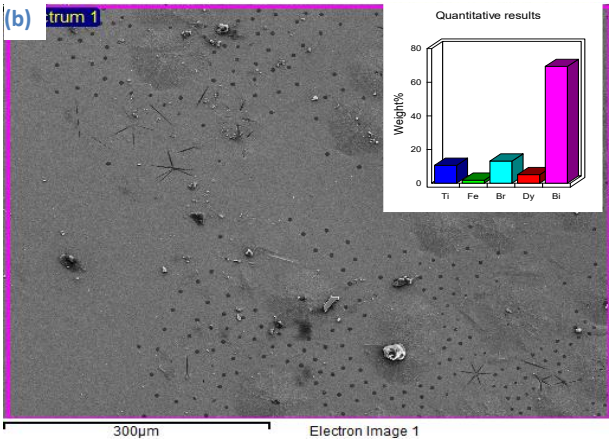

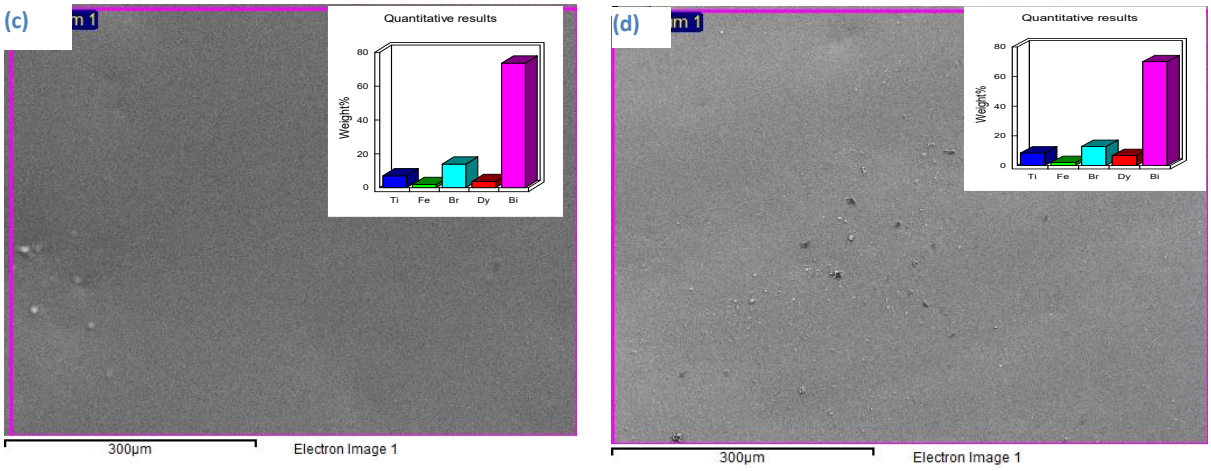

Fig 2 (a-d) SEM photographs of (100-x) BBF+ x (BDT), where x = 30, 40, 50 and 60 wt.%

Fig. 2 (a-d) shows the SEM pictures of all the glass-matrix samples. Pictures confirm that the glass composition is speeded uniformly with traces of BDT ceramic. Fig. 2a clearly shows that the BDT is little-affected on the surface. As the concentration of BDT increases, the random crystalline phases on the surface are seen as unreacted phases on the surface morphology. From this it is concluded that the possibility of a crystalline phase can be established by increasing the BDT concentration.

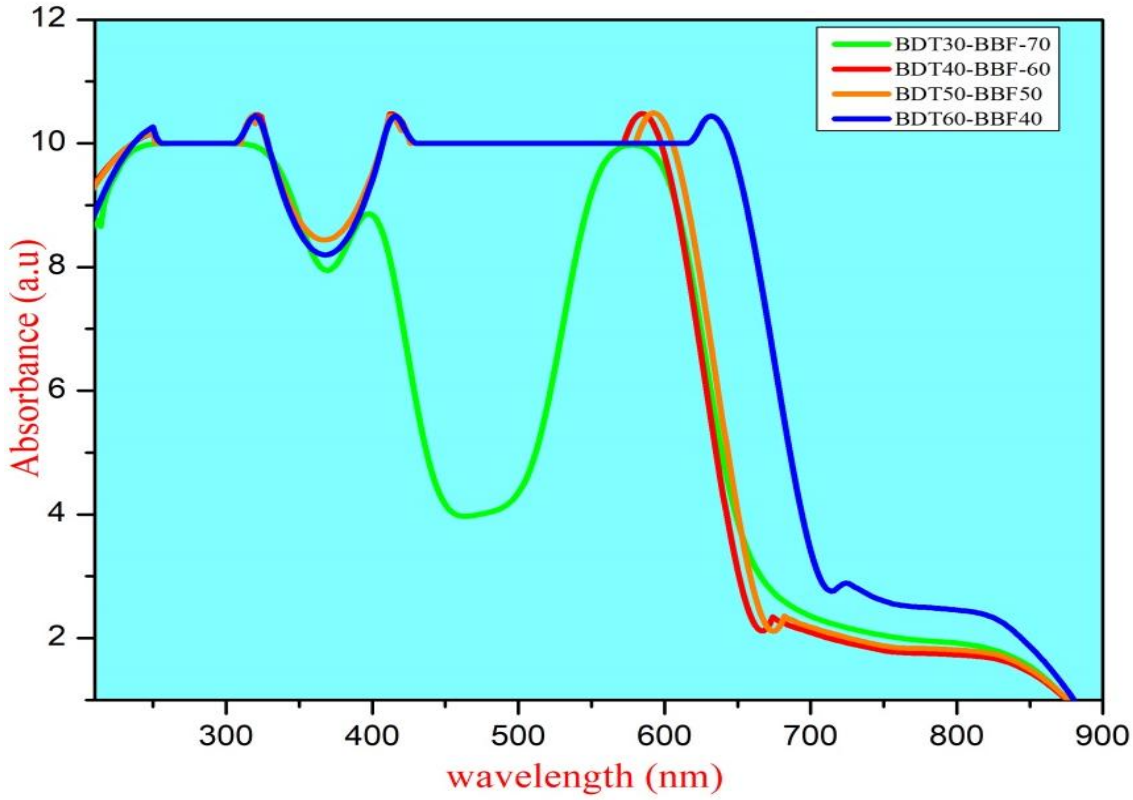

Figure 3(a): Optical absorbance vs wavelength for (100-x) BBF+ x (BDT), where x = 30, 40, 50 and 60 wt.%

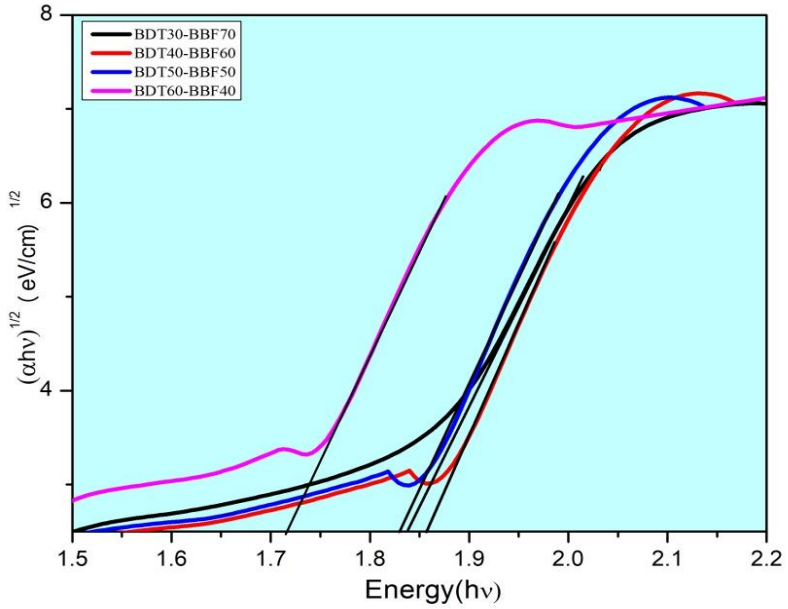

Fig 3 (b) :(hν)$^{1/2}$ vs. wavelength for (100-x) BBF+ x (BDT), where x = 30, 40, 50 and 60 wt.%

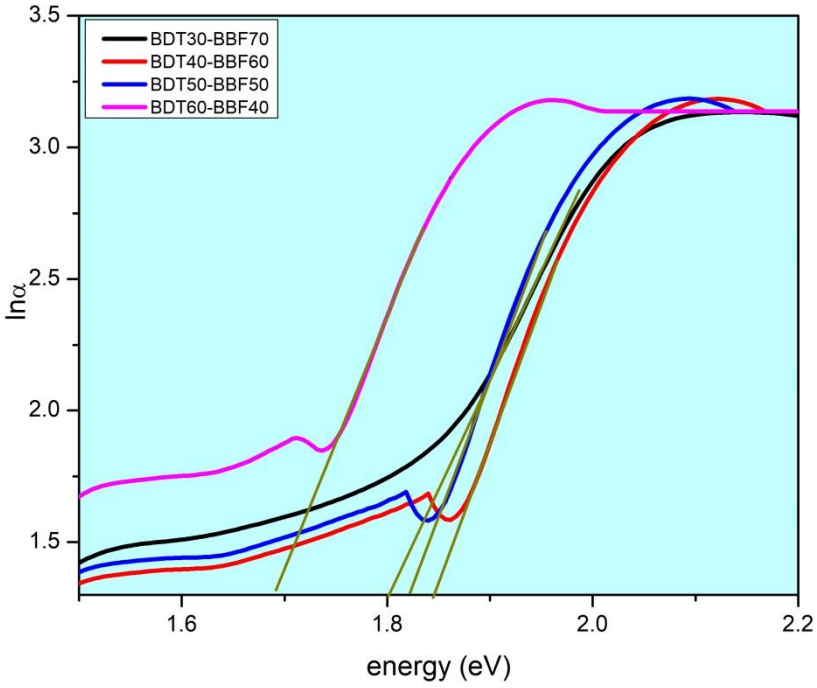

Fig 3c. Ln vs Energy for (100-x) BBF+ x (BDT), where x = 30, 40, 50 and 60 wt.%

Figure 3 (a-c) shows the optical absorbance spectroscopy through the plot of absorption against the wavelength in the UV-visible (200 nm-900 nm) region. It can be seen that the sample with the composition (100-x) BBF+ x (BDT), x=30 wt.% i.e.70 BBF+30 BDT has shown multiple absorption bands with the sharp decline in the absorption in the wavelength range (400 – 600 nm). With the increase in the BDT concentration, this absorption band disappeared and shifted towards the lower edge wavelength (or red shifted). The absorption band appearing at 450 nm is attributed to the iron transition between the two-oxidation states, namely Fe^{3+} and Fe^{2+} metal ions. This absorption is called d-d orbital electron transition in the glasses. Slight shift observed near 650 nm is attributed to the minimized defects of the sample. A sharp peak observed near the edge wavelength of 410 nm could be due to free-charge carrier absorption or non-bonding electron transitions. This is attributed to the hopping conduction process between $Fe2^{+}$ and Fe^{3+} states, through an electron. The amount of oxygen states of Fe ion was found to

be reduced on account of Dy and Bi ion substitutions in BDT in the glass-matrix helping the decrease in the Fe^{2+}/Fe^{3+} concentrations.

The absorption coefficient α was calculated from Beer- Lambart's law:

$$\alpha = \frac{1}{L}[\log(\frac{Io}{I})] \quad (6)$$

where I_O and I are the intensities of light absorbed and transmitted by the sample of thickness L. The optical energy band gap (E_{opt}) was calculated from the well-known Tauc relation given by:

$$\alpha h\nu = B(h\nu - E_{opt})^{\gamma} \quad (7)$$

B is called the band edge sharpness constant or proportionality constant, which is associated with the type of electronic transitions and is independent of energy. Based on the value of γ=1/3, 1/2, 2 one can correspond the transitions as forbidden, direct allowed, indirect allowed, indirect forbidden transitions respectively. The term hν represents the incident photon energy in eV. The variation of $(\alpha h\nu)^{\gamma}$ with hν, known as Tauc plot, for both γ=1/2 and 2 is shown in Fig. 3b and Fig. 3c respectively. The optical energy band gap was calculated by extrapolating the linear part of the graph onto the x-axis of the Tauc plot. The optical energy band gap values were summarized in Table 2. The optical band gap of higher BDT concentration of glass matrix has shown lower value compared to the other samples. This is attributed to the structural changes that took place during the introduction of BDT in the glass matrix. Based on the nature of the plots, it is evident that the present glass-matrix favors indirect transition systems. A graph drawn between energy and log (Fig. 3c) obeys the following empirical Urbach rule.

$$\alpha(\vartheta) = \beta \exp(\frac{h\vartheta}{E}) \quad (8)$$

Here, β represents a constant and E is the Urbach energy. The value of Urbach energy was determined from the reciprocal of the slopes of the liner region. The calculated Urbach energy values were summarized in Table 2. A decrease in Urbach energy is found with an increase of BDT concentration. Based on the Davis and Mott conclusions in similar ferroelectric-based glass ceramics, it is confirmed that the present BDT-based glass matrix belongs to an amorphous-semiconducting nature [24-26]. From the results it is evident that the addition of BDT to the glass matrix favors decrease in the defect concentration. Small values (>0.5 eV) suggest an inclination towards the local order and dielectric nature of the sample. A relation between the dielectric constant and the refractive index is given in the following relation:

$$\frac{(n^2-1)}{(n^2+2)} = 1 - \sqrt{\frac{Eg}{20}} \quad \text{and } n^2 = \epsilon \quad (9)$$

Molar Refractive index R_m can be obtained using the relations:

$$R_m = \frac{(n^2-1)}{(n^2+2)} * V_m \quad (10)$$

Where V_m is the molar volume. Metallization criterion (M) and electronic polarizability (α_m) can be calculated from the following relations:

$$\alpha_m = \frac{3}{4\pi N} * R_m \quad (11)$$

$$M = 1 - \left(\frac{R_m}{V_m}\right) \quad (12)$$

Where N is the Avogadro's number. The metallization criterion gives information about the non-metallic nature of the matrix. The above said parameters were calculated based on the relation given in Table 2 and Table 3.

Sample	**Refractive index (n)**	**Dielectric constant (ε)**	**Molar Refractivity (R_m)(m^3/mol)**	**Metallization Criterion (M)**	**Electronic Polarizability (α_m) ($C.m^2.V^{-1}$)**
BDT30 + BBF70	2.612	6.823	68.8	0.256	$2.48x10^{-23}$
BDT40 + BBF60	2.61	6.81	76.4	0.256	$2.76x10^{-23}$
BDT50 + BBF50	2.63	6.92	86.29	0.252	$3.12x\ 10^{-23}$

BDT60 + BBF40	2.667	7.113	90.6	0.248	3.27×10^{-23}

Table-3. Refractive index (n), Dielectric constant (ε), Molar refractivity (R_m), Metallization criterion (M) and electronic polarizability (α_m) for all the glass-matrix

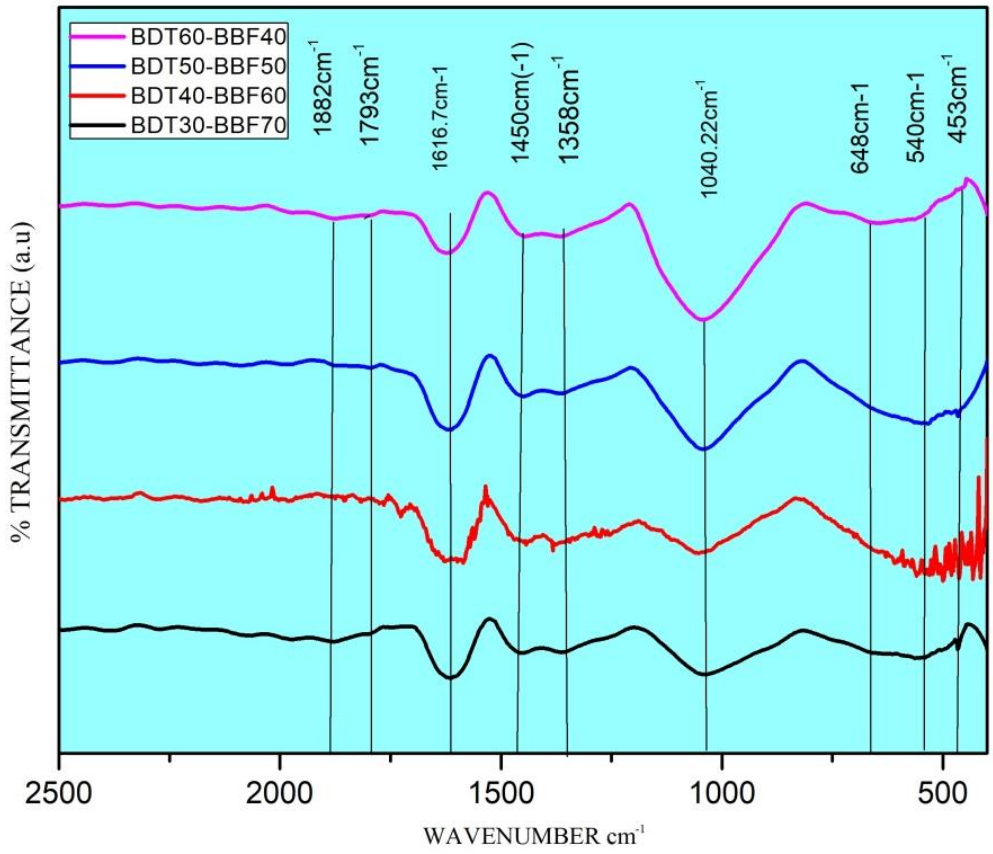

Fig 4 FTIR spectrum for (100-x) BBF+ x (BDT), where x = 30, 40, 50 and 60 wt.%

The FTIR transmission spectra of the glasses were recorded in the range of 400 to 2500 cm^{-1} and shown in Fig 4. The bands reveal the ordering of the fundamental structural units. In the present study, we observed bands I three regions. FTIR transmission minimum represent the absorption of light and gives information about the structure and functional groups of the glass-network. The first band observed between 540 and 650 cm^{-1} is attributed to the bending vibrations of B-O-B network. The second region of bands observed in the region of 800 to1000 cm^{-1} is being attributed to the stretching BO_4 units [27-28]. The bands observed in the region 1450-1600 cm^{-1} are ascribed to BO_4 units. These bands are found to increase with increasing the BDT composition. The fractional amount of BDT (N_{BDT}) can be characterized by the relation, $N_{BDT} = \frac{BO4}{BO4+BO3} * (B_2O_3+Dy_2O_3)$. From this relation it is evident that the transformation from a glassy nature to a glass-matrix increases with the incorporation of BDT. The results are consistent with SEM pictures (Fig 2). The strong broad band centered at 1040 cm^{-1} is found to increase with increasing the BDT in the matrix. Appearing more valley-like behavior in this region (with an increase in BDT concentration) can be attributed to normal vibrations of tri-, tetra- and penta- borate groups.

Fig. 5 (a-d) shows the room temperature Raman spectra for all the glass-matrix samples. The modes of vibrations were estimated by the deconvolution of the spectra. More broadening of peaks for low concentration of BDT or high concentration of glass-matrix, is considered to be the characteristics of the structural disorder associated with the glasses. The Raman spectra

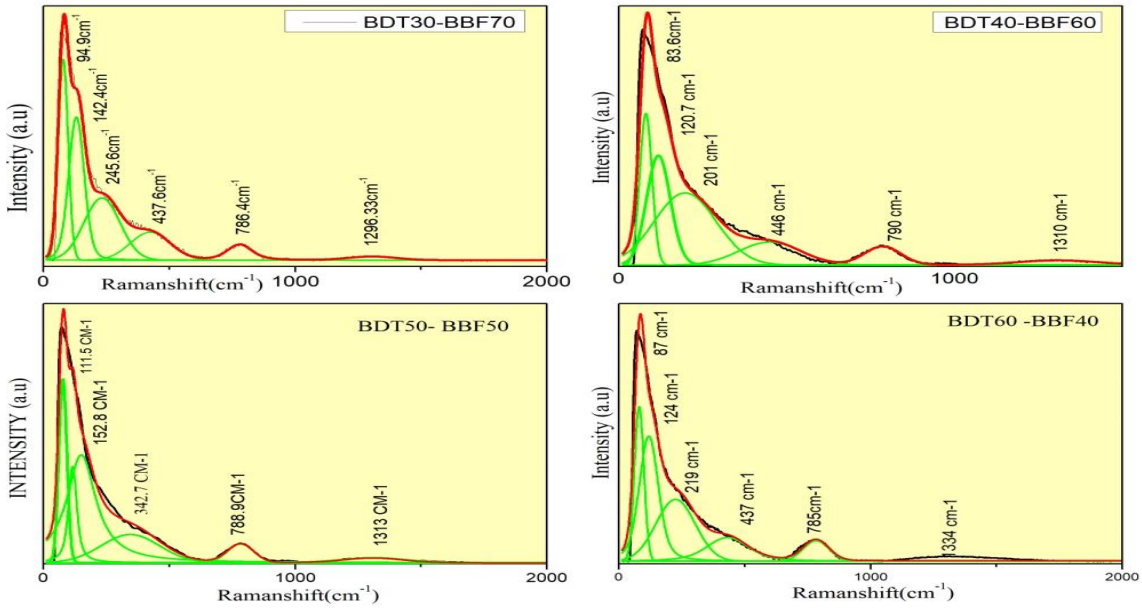

Fig 5 shows Raman spectrum for (100-x) BBF+ x (BDT), where x = 30, 40, 50 and 60 wt.%

obtained in the range of 100-2000 cm^{-1} is classified into two regions, namely below 750 cm^{-1} and above 750 cm^{-1}. The modes observed below 750 cm^{-1} is ascribed to the heavy metal cation and above 750 cm^{-1} are ascribed to the bismuth-borate network [29]. The bands observed below 750 cm^{-1} is ascribed to the vibrational modes of ordered micro-regions of the glass-matrix. Peaks observed below 150 cm^{-1} is attributed to the heavy metal ions like Bi^{3+} in BiO_6 octahedral units [27]. A slight variation in the peak position is due to the superimposed by the vibrations of Dy^{3+} ions. The Raman peak near 337 cm^{-1} is due to the vibration of Bi-O-Bi. A change of peak position is ascribed to the addition of BDT in the glass matrix. A broad Raman peak observed near 790 cm^{-1} is attributed B-O-B vibrational modes of BO_3 triangular units. A Raman peak appearing near 1300 cm-1 indicates the presence of B-O-B and B-O vibrational modes in the bismuth-borate group. Moreover, with increasing the BDT content, the peak maximum position is found to shift towards the higher wavelength region. This kind of Raman peak shifting can be ascribed to the effect of structural modification during the glass-ceramic mixed matrix formation.

The radiation-shielding property of a material is definitely contingent upon its high atomic number and high-density values. Fig. 6a demonstrates the mass attenuation coefficient (MAC) of the all glass-matrix samples against gamma-energy in the range of 10 keV to 10 MeV.

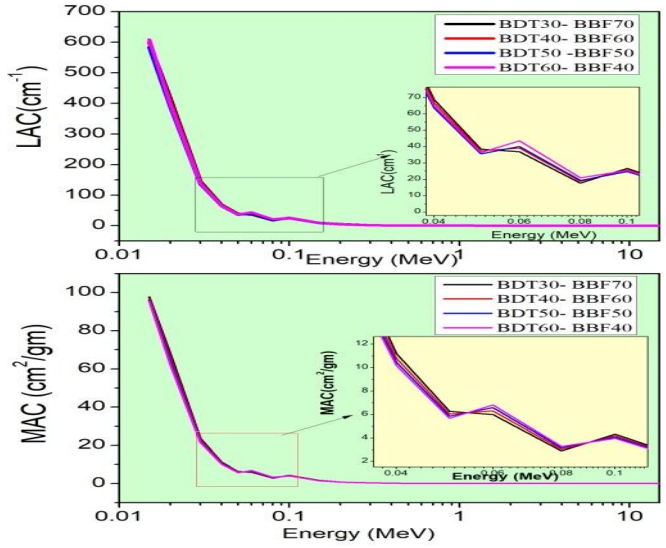

Fig 6a,6b Represents variation of LAC and MAC with photon energy for all the glass-matrix.

MAC is found to be higher at lower at higher incoming photon energy and become higher at lower photon energy. Kinks or slope changes are observed in the MAC plot in the intermediate energy range (30 to 100 keV) is shown inset Fig. 6a. From this it is evident that the BDT substitution in the glass matrix certainly improves the shielding abilities. Linear attenuation coefficient (LAC) against energy is shown in the Fig 6b. The nature of both MAC and LAC are the same, but LAC plots have shown more pronounced results. A noteworthy aspect of the kinks or slope changes observed in the intermediate energy levels (10 keV-10 MeV) is due to the mastery of the photoelectric impact. Furthermore, at higher energy regions, photoelectric absorption reduces and therefore small variation is observed in both MAC and LAC. To explore more information about the impact of BDT on the glass matrix, half vale layer (HVL) and photon mean free path (MFP) were analyzed based on the following relations:

$$MFP = \frac{1}{LAC} \quad (13)$$

$$HVL = \frac{0.693}{LAC} \quad (14)$$

The variation of MFP with energy is shown in Fig. 6c. The variation of HVL with the energy along with the DBT composition is shown in Fig. 6d. From the plots, it is evident that both

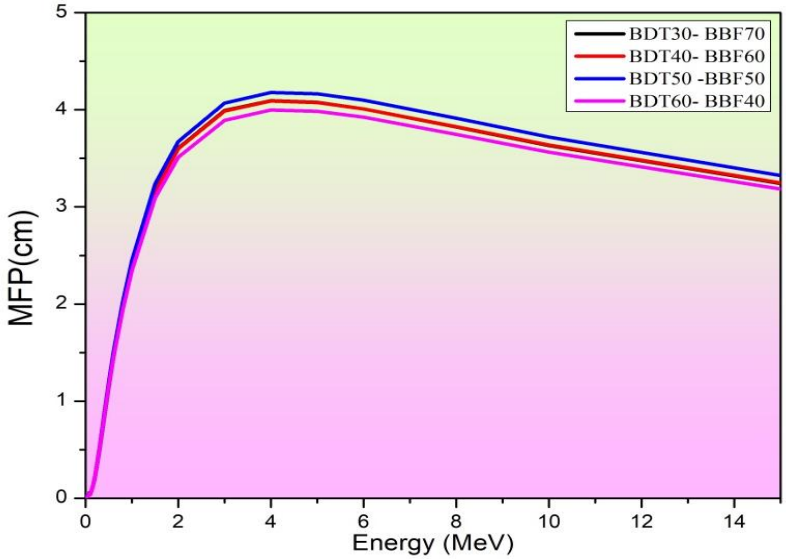

Fig 6 (c) Variation of MFP with photon energy for all the glass-matrix

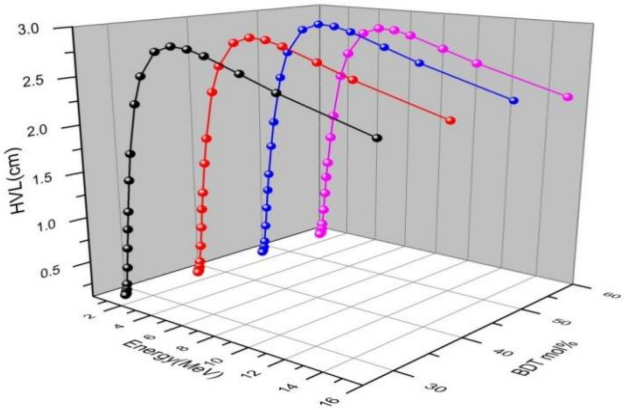

Fig 6 (d) Variation of HVL with photon energy with BDT wt.%.

MFP and HVL have smaller values at lower energies, and then increase with the increment of photon-energy. Since the values of both HVL and MFP differ inversely with the density of the glass-matrix, these materials possess inherent good gamma ray competence. These results were found to be consistent to the earlier reports [30-31]. It is also evident from Fig 6c that the higher concentration substituted BDT in the glass matric (60BDT-40BBF) has shown lower HAL value. Therefore, this glass matrix has a better gamma

ray protection competence, compared to other glass-matrix samples. Since the prepared glass-ceramics have reactant elements like Bi, Fe, Dy and O, a plot is drawn between the effective mass number (Z_{eff}) and

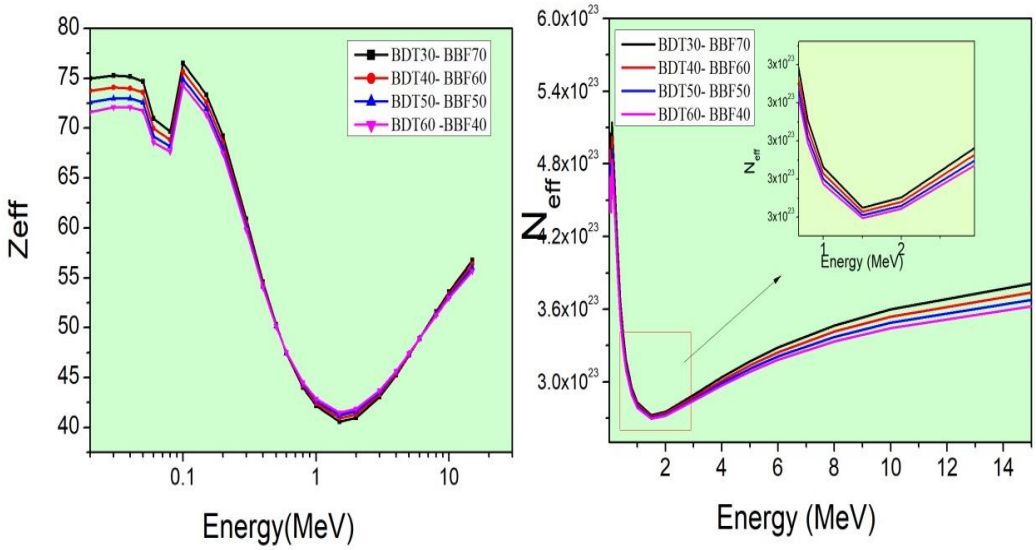

Fig 6 (e) Variation of N_{eff} and Z_{eff} with photon energy for all glass-matrix

photon energy, shown in Fig. 6e. As Z_{eff} is dependent on the photon energy, Z_{eff} decreases with the photon energy up to 2 Mev and thereafter it increases. This kind of discrepancy is attributed to the photoelectric absorption and overall atomic cross-section of the different elements. The higher effective atomic number of these glass matrices after 1 MeV, the effective photon interactions occur and result in the generation of more electrons, thereby increasing the effective electron density. It is vivid that the Z_{eff} is high at low photon energies, and as it increases Z_{eff} values drop rapidly up to 1MeV and then slightly increase. Based on this nature the present glass-matrix is considered to be switching gamma ray absorbers, unlike glasses.

4. CONCLUSIONS:

The optical and structural investigation was made on (100-x) [0.7 Bi_2O_3-0.2B_2O_3 0.1Fe_2O_3] + x [$Bi_{3.25}Dy_{0.75}Ti_3O_{12}$]; with x=30,40,50,60 wt.%. glass-matrix samples. The XRD pattern of all the samples reveals the amorphous and crystalline phases. The introduction of BDT into the glass matrix leads an increase in both glass density and molar density. From this it is concluded that there is a conversion from bridging oxygen (BO) to non- Bridging oxygen atoms (NBO) in the glass matrix. Raman peak shifting is ascribed to the effect of structural modification during the glass-ceramic mixed matrix formation. The same results were seen in FTIR plots. The 3D plot of HVL shows a decrease in trend with the increase in photon energy. Generally, materials which have high shielding properties have low values of MFP and HVL. The gamma radiation portrayal shows that the values of MFP and HVL are low initially where the shielding is more. As the photon energy increases, these values sharply increase in the energy range (2MeV-4MeV) further it slightly drops. It is noteworthy that a composition with higher BDT concentration has lower MFP values and has more penetrating power for gamma rays, making (BDT-60 BBF-40) the potential candidate for radiation shielding.

Acknowledgements: The research work is partially funded by the grant of the OU-DST-PURSE Program, India.

REFERENCES:

1. Davis, M.J., Zanotto, E.D, 2017,: "MRS Bulletin" 42,pp 195–199.
2. M. I. Ojovan and W. E. Lee, 2005,:Elsevier
3. Manuel Pedro Fernandes Graca and Manuel Almeida Valente., 2017,:MRS bulletin 42,pp213-219
4. Graca M.P.F., Silva M.G.F., Sombra A.S.B. and Valente M.A, 2008,:" Journal of Non Cryst.Solids" 354,3408.
5. Liu.J, Chen. M, Mei .X.A., Sun.Y.H and Haung. C.Q, 2012,: "Journal of Key Engineering Materials"492,pp226-229.

6. Cai.Y.H, Mei.X.A, Chen.M, Su. K.L, An. W.K and Liu.J, 2008: "Journal of Key Engineering Materials"368-372, pp 88-90.
7. Navanan Thongmee, Anucha Watcharapasron and Sukanda jiansirisomboon, 2014: "Taylor and Francis"458:1, pp 76-82.
8. Chen.M, Mei.X.A, Cai.A.H, Liu.J and Haung.C.Q, 2012: Journal of Key Engineering Materials, 492, pp 206-209.
9. Thongmee.N, Watcharapasorn.A and Jianisirisomboon.S, 2008: "Journal of Advanced Materials Research", 55-57 pp. 837-840.
10. Mohammed Abdul Basheer, Vagmare Gangadhar, Guduru Prasad, Gobburu Subramanya Kumar and Nandiraju Venkata Prasad, 2019: "Journal of Advanced Materials Research"1154,pp 80-90.
11. Jhansi.G, Veenachary Vadla, Rajashekar.A and Prasad.N.V, 2024: Springer Nature Link, 130(938).
12. Ding.Z.Z, et al, 2019: "Journal of Ceramics International."
13. Venkatesh.V, Sreenivasu.D, Ravinder Reddy.B, Shareefuddin Md, Ramadevudu.G and V.Prasad.N, 2025: "ECS Journal of Solid State Science and Technology"14 043011.
14. Mansoor.K.Gatasheh et al.2023: "Journal of Open Chemistry"
15. Mhareb .M.H.A, et al.2024; "Journal of Nuclear Engineering and Technology" pp 4709-4715.
16. Stalin.S et al, 2020: "Journal of Ceramics International" pp-17326-17334.
17. Yasaka.P et al, 2014: "Annals of Nuclear Energy", 68, pp4-9.
18. Sanghi.L, Agarwal.S, Aggarwal.A, 2012: "Journal of Materials Chemistry and physics", 133, pp151-158.
19. Sanjay Dahiya, Ashwini Sharma, Sanjay and Kishore.N, 2014: "Archives of Physics Research" 5(1):42-50.
20. Donald.I.W, 2010: "Journal of Materials Science", 32(22), 1997, pp-5851-5887.
21. Lakhwath Singh, Vanita Thakur, Punia.R, Kundu.R.S, Anupinder Singh, 2014: "Solid State Sciences"37, pp 64-71.
22. Pascuta.P, Borodi.G, Culea.E, 2009: "Journal of alloys and compounds", 479, pp579-582.
23. Ardelean.L, Cora.S, Rusu.D, 2008, Physica B, 403, pp 3682-3685.
24. Ateyyah M.Al-Baradi, Abdel Wahab.E.A,Shaaban.Kh.S,2021: "Springer Nature B.V"
25. Shaaban. K.S, Wahab EAA, Shaaban ER, Yousuf. E.S,Mahmoud SA,2020: "Optical and Quantum electronics",52:125
26. Shaaban. K.S, Wahab EAA, Shaaban ER, Yousuf. E.S, Mahmoud SA, 2020: "journal of electronic materials".
27. Rada.S, Culea.E, Bosca.M, Muntean.R, Pascuta.P, 2007: "Vib.Spectrosc"48, pp 285-288.
28. Abdel-Khalek.E.K,Mohamed.E.A,Shaaban.M.Salem,Ebrahim.F.M,Kashif.I,2012: "Journal of Materials Chemistry and Physics",133,pp69-77.
29. Seema Thakur, Vanita Thakur, Anumeet Kaur, Lakhwant Singh, 2018: "Journal of Non-Crystalline Solids", 512, pp 60-71.
30. Gurinder pal singh, et al, 2020: "Journal of material Research and Technology".
31. Sayyed.M.I,Ashok Kumar,Tekin.H.O,Ramandeep Kaur,Mandeep Singh,Agar.O,Mayeen Uddin Khandaker,2020:118,103118.